Integrating network analysis and experimental validation to reveal the ferroptosis-associated mechanism of velvet antler in the treatment of chronic atrophic gastritis

Quan Liao [a], Zhenzhen Guo [b], Chenchun Ding [a], Renjie Zuo [a], Guoyan Liu [a,b,*]

[a] Department of Gastrointestinal Surgery, Zhongshan Hospital of Xiamen University, School of Medicine, Xiamen University, Xiamen, Fujian, China
[b] School of Pharmaceutical Sciences, Xiamen University, Xiamen, Fujian, China

Abstract

Chronic atrophic gastritis (CAG) is precancerosis with limited treatment options. This study investigated the therapeutic effects of velvet antler (VA), a traditional natural medicine, on CAG, with a focus on ferroptosis. *In vivo* experiments demonstrated the efficacy of VA in alleviating CAG, and network pharmacology analysis revealed its involvement in related terms, including inflammation, oxidative stress, and cell proliferation. Analyses further confirmed the modulation of ferroptosis by VA, particularly via the Keap1-Nrf2/HO-1/GPX4 pathway. *In vitro* assays supported these findings, demonstrating the ability of VA to reduce methylnitronitrosoguanidine-induced inflammation, oxidative stress, and ferroptosis in GES-1. This study provides a basis for exploring VA as a potential treatment for CAG, and offers new therapeutic strategies targeting ferroptosis.

Keywords: Chronic atrophic gastritis, Ferroptosis, Network analysis, Velvet antler

1. Introduction

Chronic atrophic gastritis (CAG) is precancerosis characterized by progressive replacement of normal glandular structures with fibrous tissues or aberrant epithelia during chronic inflammation. This transformation leads to marked atrophy of gastric mucosal epithelium and glands. Annually, CAG presents a 0.1%−0.3% risk of progression to gastric adenocarcinoma [1]. Notably, mucosal damage reversal is possible in approximately 20% of CAG cases following eradication of the underlying cause, such as *Helicobacter pylori* infection [2]. However, in most cases, the mucosal damage is irreversible [3].

Recently, ferroptosis has been involved in the etiology of diseases spanning the digestive, cardiovascular, neurological, and urological domains [4,5]. Emerging evidence indicates that reactive oxygen species (ROS) plays a critical role in CAG pathogenesis [6]. Chronic inflammation in CAG increases ROS levels, leading to enhanced lipid peroxidation, which is a key trigger for ferroptosis [7]. The resultant cell death not only exacerbates tissue damage but also further amplifies oxidative stress, establishing a vicious cycle that contributes to the gastric mucosal atrophy and increases the risk of neoplastic transformation. Emerging evidence suggests that ferroptosis is involved in CAG pathogenesis, making it a potential target for therapeutic intervention [8]. Guo et al. reported that the YY1/miR-320a/TFRC signaling pathway can improve CAG by enhancing fserroptosis [9]. Zheng et al. reported that AGEs-RAGE signaling performs a similar function [7].

Velvet antler (VA), an undeveloped antler of cervids such as the sika or red deer, is prized in several

Received 6 December 2024; accepted 18 April 2025.
Available online 13 June 2025

* Corresponding author at: School of Medicine, Xiamen University, Xiamen, Fujian 361000, China.
E-mail address: liuguoyan@xmu.edu.cn (G. Liu).

https://doi.org/10.38212/2224-6614.3546

cultures for its nutritional and multifunctional properties, which are attributed to its rich composition of bioactive components. Several studies have isolated and determined the chemical components of VAs, including amino acids, peptides, proteins, lipids, saccharides, fatty acids, phospholipids, inorganic substances, and minerals [10]. It has diverse pharmacological benefits, including anti-inflammatory [11,12], antioxidant [13], anti-cancer [14], and wound healing [15] effects. For example, Liu et al. reported that the VA methanol extract has anti-neuroinflammatory activity in lipopolysaccharide-stimulated macroglia [16]. Wang et al. reported that VA significantly increased oxidative stress resistance of *Caenorhabditis elegans* treated with juglone [13]. Therefore, VA is a promising candidate for treating CAG.

Network pharmacology is a modern approach that combines database analysis with biological system modeling to predict complex drug-target interactions [17]. Recently, several natural medicinal studies have used this method. For example, Sun et al. revealed the effects of the Wuzang Wenyang Huayu decoction on dementia [18]. By leveraging network pharmacology, we identified the therapeutic potential of VA against CAG in animal models. Subsequent network pharmacology predictions of the VA-CAG target interactions were validated at the cellular level, thereby enhancing the reliability and predictive power of this methodology.

Abbreviations

CAG	chronic atrophic gastritis
VA	velvet antler
GO	gene ontology
KEGG	kyoto encyclopedia of genes and genomes
MNNG	methylnitronitrosoguanidine
PGE2	prostaglandin E2
HED	human-equivalent dosage
RED	rat equivalent dose
LVA	low-dose velvet antler
HVA	high-dose velvet antler
VTE	vitacoenzyme
ALT	alanine aminotransferase
AST	aspartate aminotransferase
BUN	blood urea nitrogen
TEM	transmission electron microscope
ELISA	enzyme-linked immunosorbent assay
H&E	hematoxylin and eosin
PPI	protein–protein interaction
GES-1	human gastric epithelial cells line
CCK8	cell counting Kit-8
ROS	reactive oxygen species
SOD	superoxide dismutase
MDA	malondialdehyde
BSA	bovine serum albumin
BP	biological Process
CC	cellular Component
MF	molecular Function
DEP	differentially expressed proteins

2. Materials and methods

2.1. Preparation of VA crude extract

VA powder was sourced from Shuangyang Deer Farm (Jilin, China), using previously described extraction methods [13]. VA powder (1 g) was dissolved in 30 mL of methanol (HPLC-grade, Aladdin, Shanghai, China) and ultrasonicated (40 kHz, 25 °C) for 1 h in an ultrasonic bath. Then centrifuge the mixture at 8000 *g* to separate insoluble components. Collect supernatant and evaporate methanol solvent (0.09 MPa) at 40 °C using a rotary evaporator. The resulting extract was stored at −20 °C.

2.2. Animals

This study was approved by the Animal Ethics Committee of Xiamen University (Approval No. XMULAC20240028) and strictly adhered to approved protocols. Forty male Sprague-Dawley rats (eight weeks old) were procured from Vital River Biotechnology Co., Ltd. and acclimatized at the Xiamen University Laboratory Animal Center for a week prior to experimentation.

The daily human-equivalent dosage (HED) of VA powder was 6 g/d (assuming an adult weight of 70 kg). Dosage conversion from rats to humans was determined using the body surface area normalization factor (Km). Based on body surface area conversion [19], the rat equivalent dosage (RED) was calculated to be 530 and 265 mg/kg/day for the high-and low-dose groups, respectively. The dosage was calculated as follows:

$$\mathrm{HED} = \frac{6}{70} \approx 0.086\ \mathrm{g} \Big/ \mathrm{kg}$$

$$\mathrm{Rat\ Km} = 6, \mathrm{human\ Km} = 37$$

$$\mathrm{RED} = \frac{\mathrm{HED}}{\left(\mathrm{rat\ Km}/\mathrm{human\ Km}\right)} = 0.53\ \mathrm{g} \Big/ \mathrm{kg}$$

The rats were allocated to five groups (n = 8): CAG model, low-dose VA (LVA), high-dose VA (HVA), vitacoenzyme (VTE), and control. For CAG induction, methylnitronitrosoguanidine (MNNG,180 μg/mL; Meilunbio, Dalian, China) was added to the drinking water for 12 weeks. Subsequently, VA,

VTE, or saline (control) was orally administered daily for four weeks. After treatment, rats were euthanized under isoflurane anesthesia for stomach tissue collection. Part of the stomach was fixed, and part was stored at −80 °C.

2.3. Enzyme-linked immunosorbent assays (ELISA)

TNF-α and IL-6 in the serum and cell culture supernatants were determined by specific assay kits (NeoBioscience Technology Co., Ltd., Shenzhen, China). Serum PGE2 levels were determined using ELISA kits (Solarbio Technology Co., Ltd., Beijing, China).

2.4. Hematoxylin and eosin (H&E) staining

Gastric tissues were fixed, embedded, sectioned, and stained using an H&E kit (Servicebio Technology Co., Ltd., Wuhan, China), followed by microscopic examination (Olympus, Tokyo, Japan).

2.5. Toxicity assays

Alanine aminotransferase (ALT), aspartate aminotransferase (AST), and blood urea nitrogen (BUN) (Jiancheng Bioengineering Institute, Nanjing, China) were measured. ALT and AST were measured at 505 nm, whereas BUN was measured at 640 nm after incubation at 37 °C.

2.6. Network and functional enrichment analysis

The ingredients of VA were identified in the BATMAN-TCM and HERB databases, with "LU RONG" as the search term. Compounds were screened using swissADME with a score of "high" for gastrointestinal absorption and at least two "yes" for druglike-ness. Target predictions were conducted using SwissTargetPrediction, with CAG targets identified from the GeneCards and DisGenet databases. Intersections of VA and CAG targets were performed to identify common targets for Gene Ontology (GO) and Kyoto Encyclopedia of Genes and Genomes (KEGG) using DAVID and visualized using bioinformatics tools.

2.7. Analysis of common target genes

Protein–protein interaction (PPI) networks were built in STRING and Cytoscape software (version 3.10), incorporating ferroptosis-related data from the FerrDb V2 database.

2.8. Molecular docking validation

Protein targets and VA chemical component structures were acquired from PDB and PubChem databases, respectively. Docking simulations were performed using AutoDockTools (version 1.5.6), and PyMOL (version 2.5.5) was used for visualization.

2.9. Cell viability

Human gastric epithelial cells (GES-1) were cultured in RPMI-1640 medium with 10% serum, cultured at 37 °C and 5% CO_2 to ensure optimal growth conditions. GES-1 were seeded with 1×10^4 cells/well in 96-well plates. After treatment, the supernate in each well was replaced with a 1:9 mixture of the CCK8 reagent (Lablead Biotechnology, Beijing, China) and fresh medium, followed by incubation for 1.5 h. Results were measured at 450 nm to calculate cell viability.

2.10. Detection of ROS

GES-1 were cultured in 6-well plates with 3×10^5/well. Following treatment, DCFH-DA (Lablead Biotechnology, Beijing, China) was prepared in serum-free medium (1:1000 dilution). GES-1 were treated with DCFH-DA solution in the cell incubator. ROS-induced fluorescence was quantified using flow cytometry (Attune Nxt, Thermo Fisher Scientific, Waltham, MA, USA).

2.11. Transmission electron microscope (TEM)

GES-1 were fixed, dehydrated, and embedded in epoxy resin. Sections were mounted on grids and stained. Mitochondria were observed and imaged using a TEM (JEOL, Tokyo, Japan).

2.12. Oxidative stress markers

Rat blood was centrifuged at 1500 *g* to obtain serum. Superoxide dismutase (SOD) and malondialdehyde (MDA) were determined by specific assay kits (Beyotime Biotechnology, Shanghai, China). SOD was measured at 450 nm and MDA was measured at 535 nm.

2.13. Iron assay

GES-1 were incubated with FerroOrange (1 μmol/L, Dojindo, Japan) for 30 min at 37 °C in a 5% CO_2 atmosphere. Fluorescence microscopy (Zeiss, Oberkochen, Germany) was utilized for visualization.

2.14. Western blot

GES-1 was lysed in RIPA containing a protease-inhibitor cocktail (Yeasen Biotechnology, Shanghai, China) on ice. Supernatant was collected after centrifugation. Proteins were mixed with loading buffer, denatured by boiling, and separated on gels. Bands were transferred to PVDF membranes, blocked and incubated with antibodies overnight, followed by secondary antibodies for 1 h, and bands were observed. ImageJ was used to quantify band intensities. To ensure consistency, density was measured and normalized to that of the corresponding control. The relative protein expression levels were then calculated.

Antibodies from Proteintech against the following proteins were used for immunoblotting: PTGS2 (cat#66351-1-Ig, 1:2000), GPX4 (cat#67763-1-Ig, 1:2000), NRF2 (cat#16396-1-AP, 1:4000), KEAP1 (cat#60027-1-Ig, 1:2000), HO-1 (cat#66743-1-Ig, 1:2000), β-actin (cat#66009-1-Ig, 1:10000).

2.15. Immunofluorescence

GES-1 were seeded on coverslips in 24-well plates. GES-1 were fixed and permeabilized. Coverslips were blocked by 5% bovine serum albumin (BSA). GES-1 were treated with antibodies (1:200 in 5% BSA) overnight at 4 °C. Then they were incubated with the species-specific secondary antibodies (1:500 in 5% BSA) for 1 h. Coverslips were mounted onto slides using DAPI-containing medium to counterstain the nuclei. The coverslips were observed by a confocal microscope (Zeiss, Oberkochen, Germany).

2.16. Statistical analysis

Data were analyzed using analysis of variance (GraphPad Prism software 8.0.2). Statistical significance set at $p \leq 0.05$ was considered statistically significant. # indicates a comparison between the model and control groups and * indicates a comparison between each group and the model group.

3. Results

3.1. VA improved gastric structural damage in MNNG-treated CAG rats

H&E staining revealed extensive localized atrophy of the gastric mucosal layer, disorganized and cystically dilated glandular structures, and marked inflammatory cell infiltration within the lamina propria in the model group. In the control group, H&E staining revealed a well-organized mucosal architecture with tightly arranged glandular epithelium, intact basement membranes, and minimal inflammatory infiltration. Both the LVA and HVA groups exhibited varying degrees of improvement compared to the model group. In the LVA group, improvements were noted with reduced cystic dilation and partial restoration of the mucosal architecture, although moderate inflammatory cells remained. The HVA and VTE groups displayed pronounced restoration of normal histology, with an orderly glandular arrangement, preserved mucosal thickness, and minimal inflammatory infiltration, closely resembling the control group (Fig. 1A). These observations highlight the effectiveness of VA in alleviating the CAG-induced gastric mucosal damage. Serum ALT, AST, and BUN levels remained within normal ranges across all groups, indicating minimal side effects of treatment (Fig. S3 (https://doi.org/10.38212/2224-6614.3546)).

3.2. VA improved serum PGE2, SOD and MDA levels in vivo

Serum PGE2 levels were significantly elevated in the MNNG-induced gastritis rat model, indicating disruption in the normal biochemical processes associated with gastric inflammation. However, VA treatment resulted in a marked improvement in PGE2 levels compared to those in the model group, suggesting that VA effectively ameliorated the inflammatory response (Fig. 1B). Antioxidant therapy is essential for CAG management. SOD, a primary ROS scavenger, and MDA, a ROS byproduct and ferroptosis marker, were evaluated in rats. Compared to the model group, SOD was significantly decreased, while MDA was increased in MNNG. VA treatment substantially increased SOD and decreased MDA compared to MNNG group, with the HVA group showing superior efficacy compared to the LVA group (Fig. 1C and D).

3.3. Prediction and analysis of common targets of VA and CAG

96 VA components were identified from the BATMAN and HERB databases. Following screening, 53 potentially active components were identified after the screening (Table S1 (https://doi.org/10.38212/2224-6614.3546)). These compounds were then subjected to target prediction, which resulted in 617 targets (probability > 0). GeneCards searches using the keyword “Chronic atrophic gastritis” yielded 446

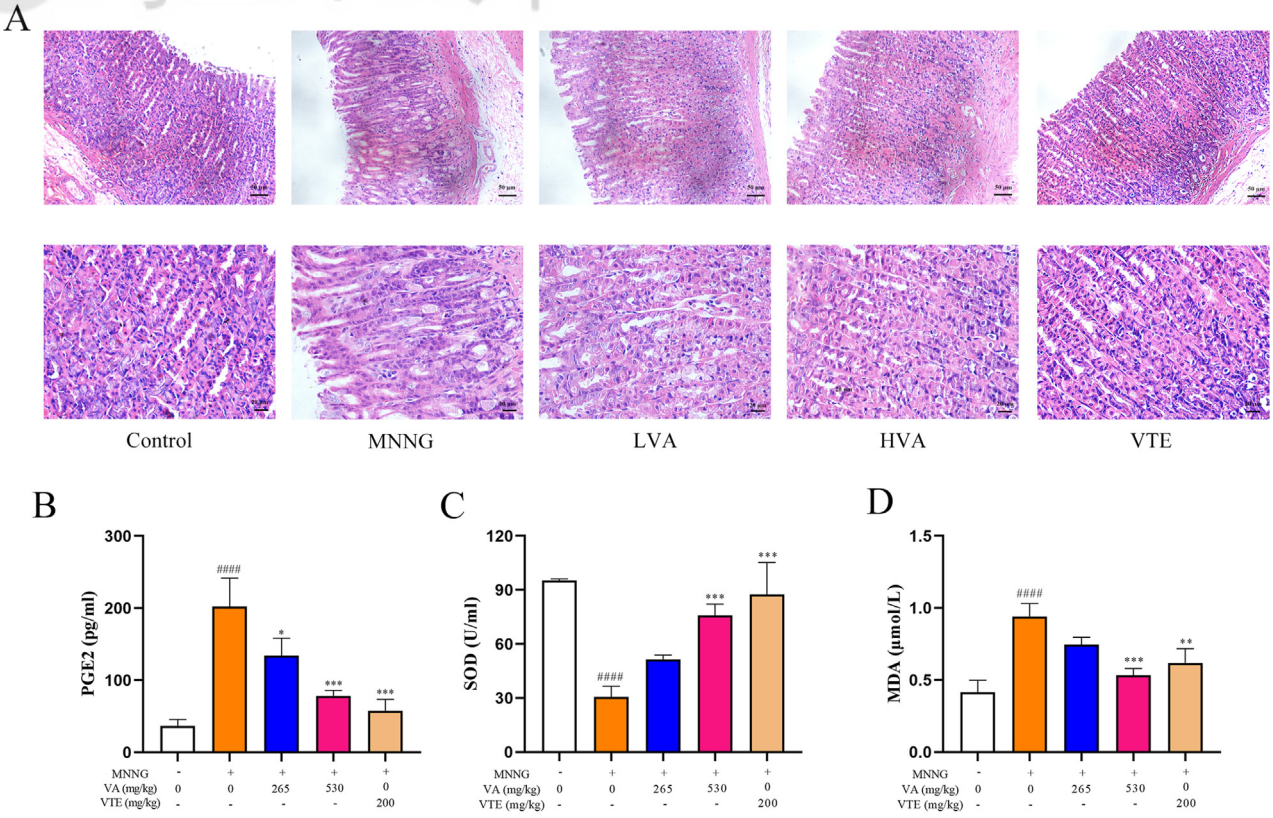

Fig. 1. Effects of VA on MNNG-induced CAG in vivo. (A) H&E staining of representative pathological changes of gastric tissue. The upper row represents low magnification (200×), and the lower row represents high magnification (400×). (B) The level of serum PGE2. (C) The level of serum SOD. (D) The level of serum MDA.

results (relevance score ≥ 7.988702774). The DisGenet search yielded 203 results (score ≥ 0.01). Removal of duplicate values resulted in the identification of 556 target genes. The Venn diagram shows 90 intersecting genes (Fig. 2A). The PPI network comprised 88 nodes and 1216 edges, indicating robust connectivity (Fig. 2B). Nineteen hub genes including TNF, IL6, AKT1, and PTGS2, were identified using the Centiscape plugin (closeness ≥ 0.006650124205376911, betweenness ≥ 67.7727272727272, degree ≥ 27.636363636363637) (Table 1).

We compared the hub genes with the ferroptosis database FerrDb and found that the majority of these genes were associated with ferroptosis, including IL6, EGFR, SRC, PTGS2, TLR4, HIF1A, PPARG, AR, and PRKCA. Among these, PTGS2 is considered a marker of ferroptosis.

3.4. Functional enrichment analysis

GO analysis revealed three aspects. Biological process (BP) revealed that the effect of VA on CAG was primarily in bacterial inflammation, apoptosis, and cell proliferation (Fig. 2D). Cellular component (CC) analysis highlighted the involvement of macromolecular complexes and extracellular regions (Fig. 2E), often associated with signal transduction, protein synthesis, and cell repair. Molecular function (MF) analysis showed increased enzyme and kinase activities (Fig. 2F), suggesting that protein kinases may be involved in some signaling pathways in this process. KEGG pathway analysis indicated that inflammation and tumor progression (Fig. 2G), were key features of chronic inflammation and carcinogenesis in CAG. The PI3K-Akt pathway was suggested to be involved. Table S1 (https://doi.org/10.38212/2224-6614.3546) lists the top ten counts for each aspect. Integration of the PPI network and KEGG results facilitated the construction of component-target-pathway networks (Fig. 2C), highlighting the interactions between the active compounds of VA, their potential targets, and their involvement in various biological pathways.

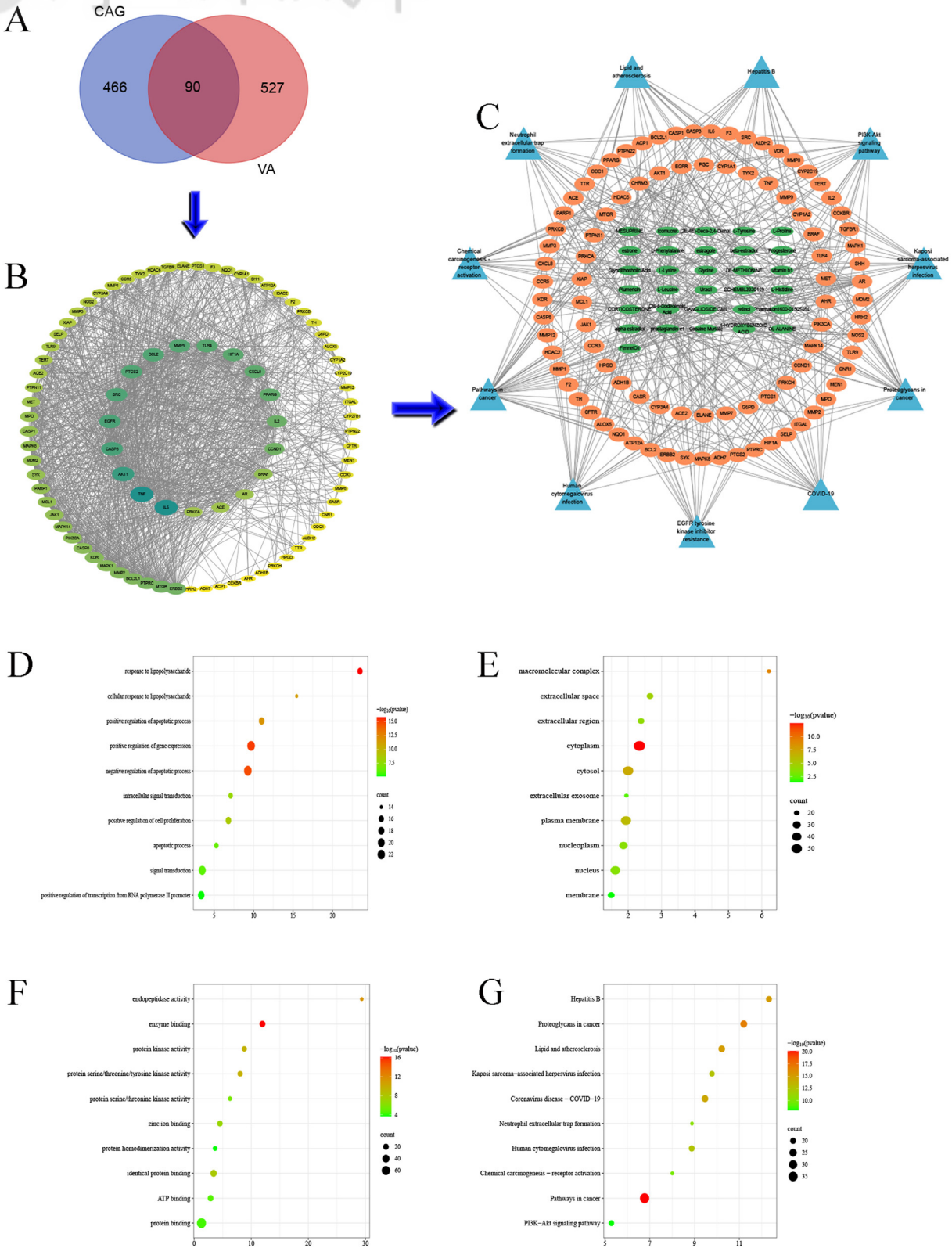

Fig. 2. Network analysis of VA against CAG. (A) Veen diagram of interaction genes between VA and CAG. (B) 19 hub genes in PPI network. (C) Component-target-pathway networks. Green nodes refer to hub genes. Orange nodes refer to intersecting genes other than hub genes. Blue nodes refer to corresponding KEGG pathway. (D–G) The top 10 enriched terms in GO and KEGG pathways.

Table 1. Centrality of hub gene computed by Centiscape.

No.	Name	Closeness	Betweenness
1	TNF	0.009709	508.607
2	IL6	0.009709	519.9331
3	AKT1	0.009009	330.3333
4	CASP3	0.008621	166.2973
5	EGFR	0.008547	198.6458
6	SRC	0.008403	519.2609
7	BCL2	0.008333	137.1324
8	PTGS2	0.008403	299.4498
9	MMP9	0.008264	128.1995
10	TLR4	0.00813	136.0193
11	HIF1A	0.00813	134.6768
12	CXCL8	0.008065	151.5886
13	PPARG	0.008065	188.2409
14	IL2	0.007752	91.86842
15	CCND1	0.007692	83.46501
16	BRAF	0.006993	80.0195
17	AR	0.006944	122.5001
18	ACE	0.006897	190.9263

3.5. Molecular docking validates relationships between components and hub genes

Molecular docking confirmed the strong interactions between the active ingredients and hub genes. An affinity of ≤ -5.0 kcal/mol indicates a interaction [20]. The higher the affinity, the less stable is the binding. Eight proteins with the highest degree values were screened and 31 components were screened in the network (Fig. 3A). Three components with the strongest binding capacity to each of the hub genes were as follows: TNF to progesterone (−8.72), corticosterone (−7.72) and estrone (−7.18); IL6 to progesterone (−6.12), estrone (−5.36 kcal/mol) and corticosterone (−5.32); AKT1 to progesterone (−8.73), SCHEMBL3330119 (−7.25) and estrone (−7.24); CASP3 to progesterone (−6.35), alpha estradiol (−6.01) and glycolithocholic Acid (−5.9); EGFR to progesterone (−8.27), retinol (−7.47) and beta-estradiol (−7.4); SRC to progesterone (−6.73), retinol (−6.71) and alpha estradiol (−6.28 kcal/mol); BCL2 to progesterone (−7.42), glycolithocholic acid (−6.85) and estrone (−6.47); PTGS2 to progesterone (−8.63), cis-4-dodecenoic Acid (−7.33) and estrone (−7.3) (Table S1 (https://doi.org/10.38212/2224-6614.3546)). The representative pairs are shown in Fig. 3B.

3.6. VA improved cell viability and mediated inflammation in MNNG-induced CAG cells

To validate the relationship between VA, ferroptosis and CAG suggested by network pharmacology analysis, we conducted *in vitro* experiments using MNNG-induced CAG models. Initially, the modeling concentration of MNNG was determined to be 20 μM after 8 h using the CCK-8 assay (Fig. S1 (https://doi.org/10.38212/2224-6614.3546)). Treatment with VA for 24 h effectively ameliorated the MNNG-induced reduction in cell viability (Fig. 4A). Additionally, VA treatment inhibited the secretion of TNF-α and IL-6 induced by MNNG (Fig. 4B and C).

3.7. VA attenuated ferroptosis in MNNG-induced CAG cells

Previous studies have implicated ferroptosis in CAG pathogenesis [8,9]. Therefore, we examined the effects of VA on ferroptosis in GES-1. VA treatment inhibited excessive ROS generation induced by MNNG (Fig. 4D) and attenuated the accumulation of ferrous ions (Fig. 5B and C). The mitochondria play an important role in ferroptosis. We used TEM to evaluate the effects of MNNG and VA on the ultrastructure. GES-1 treated with MNNG showed partial mitochondrial vacuolization, disordered arrangement of mitochondrial cristae, and blurred structure. In contrast, cells treated with VA exhibited more organized mitochondrial cristae, indicating an improvement in the morphological changes induced by MNNG (Fig. 5A). Moreover, VA treatment partially reversed MNNG-induced dysregulation of SOD and MDA levels (Fig. 5D and E), which is consistent with observations in CAG rats. PTGS2 is a ferroptosis marker [21]. Immunofluorescence analysis revealed that MNNG-induced upregulation of PTGS2 protein expression was suppressed by VA treatment (Fig. 5F).

3.8. VA inhibited ferroptosis via the Keap1-Nrf2/HO-1/GPX4 pathway

Nrf2, a classical antioxidant pathway, regulates ferroptosis. Compared to the control group, MNNG exposure led to an increase in Keap1 and HO-1 expression and a decrease in GPX4 expression. VA treatment markedly suppressed Keap1 expression and upregulated Nrf2, HO-1 and GPX4 expression (Fig. 6A–E). Immunofluorescence results revealed elevated levels of Nrf2 protein expression in VA-treated GES-1 cells, with a tendency toward nuclear localization, compared to the MNNG group (Fig. 6F and G).

4. Discussion

Gastric cancer ranks fifth in incidence and fourth in mortality [22]. CAG is mostly irreversible after the removal of the causative factors [2]. Therefore, the

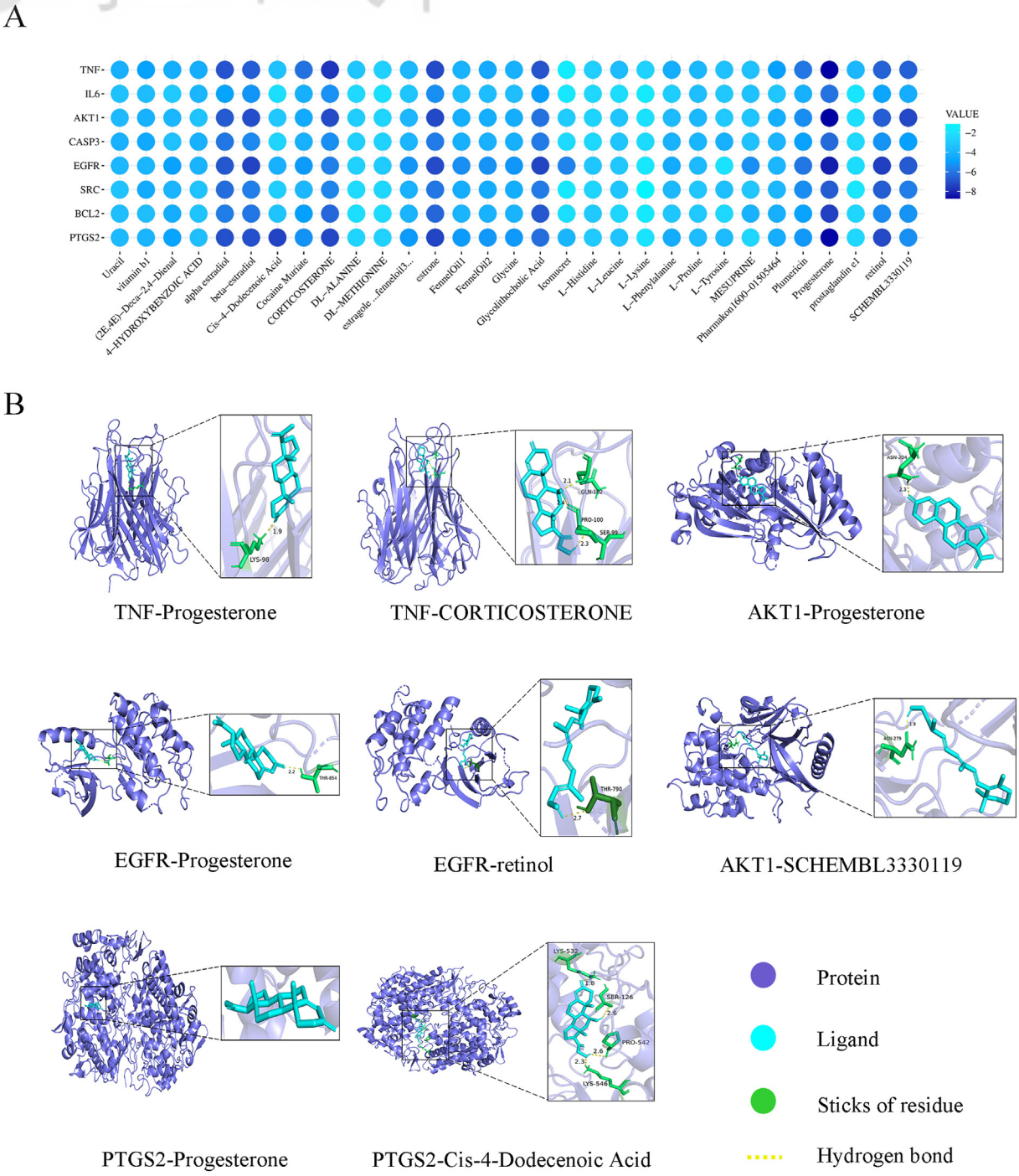

Fig. 3. Molecular docking. (A) Bubble heatmap of 8 hub genes docked to 31 components. (B) Representative docking complex.

discovery of novel CAG treatments is crucial. Our study demonstrated that VA effectively reversed MNNG-induced pathological structures *in vivo*. Network pharmacological analysis revealed a close association between VA and CAG, involving ferroptosis, which was experimentally validated. Moreover, VA mitigates MNNG-induced CAG via the Keap1-Nrf2/HO-1/GPX4 pathway, thereby offering potential therapeutic insights.

We elucidated the network regulatory mechanism of VA in CAG by identifying its targets, analyzing their implicated biological functions, and identifying hub genes using PPI screening. In MNNG-induced CAG cell models, VA enhanced cell viability,

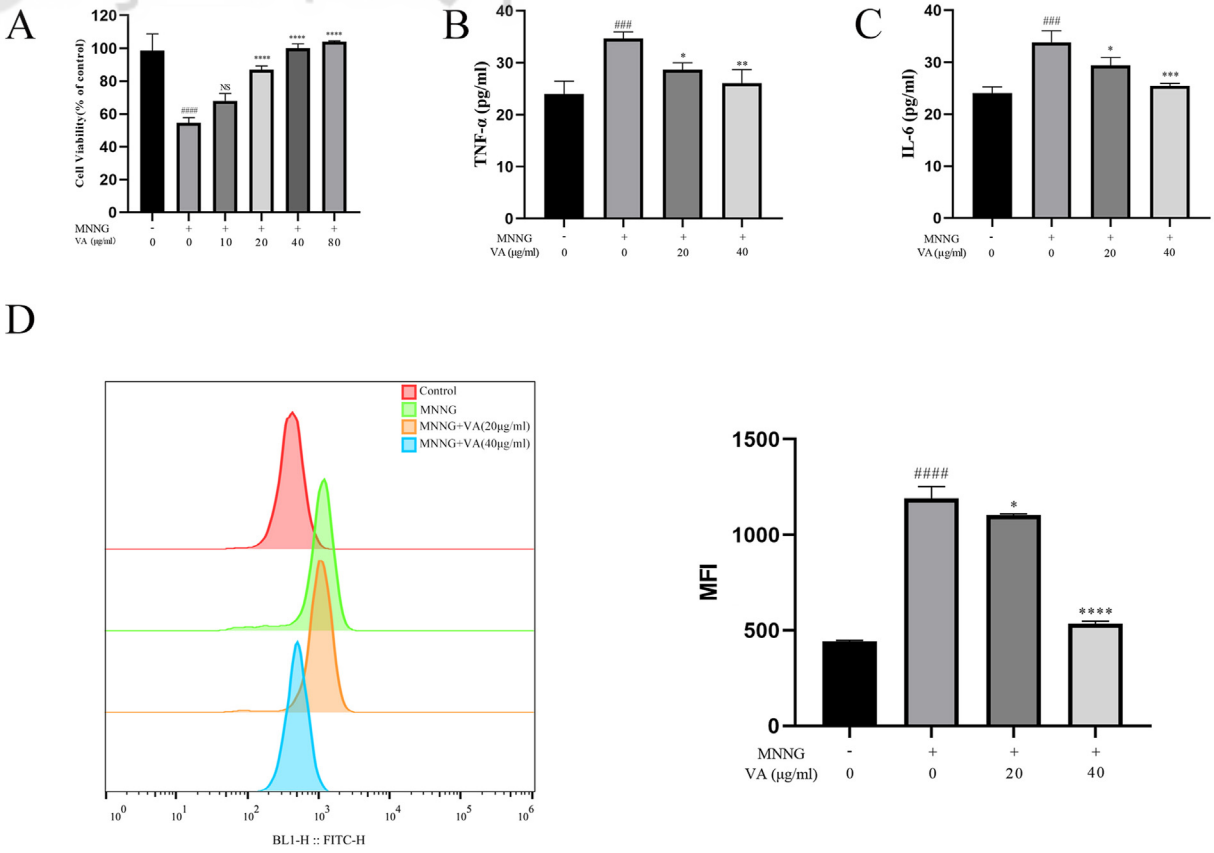

Fig. 4. Effects of VA on MNNG-induced CAG in vitro. (A) Cell viability. (B–C) The level of TNF-α and IL-6 by ELISA. (D) The levels of ROS by flow cytometer.

modulated inflammation, and improved oxidative status by inhibiting TNF-α and IL-6 secretion, consistent with the hub gene expression patterns. TNF-α and IL-6 are pro-inflammatory cytokines involved in the gastric inflammatory response [23], whereas PGE2 is a product of the cyclooxygenase pathway. Excessive PGE2 production during chronic inflammation is associated with persistent mucosal damage and precancerous lesions. Monitoring PGE2 levels helps evaluate the inflammatory state and mucosal repair mechanisms in CAG [24].

Ferroptosis has emerged as a novel target for treatment [4]. GPX4 and PTGS2 are hub genes associated with ferroptosis and regulate lipid oxidation [21,25]. Recently, several studies have reported that ferroptosis can occur during CAG [8,9]. Our comparison between hub genes and the FerrDb database revealed a close association between VA treatment and ferroptosis, consistent with the PTGS2 and GPX4 expression levels observed in our experiments. SOD, MDA and ferrous ion staining results validated this finding. Notably, hub genes such as IL6, EGFR, TLR4, HIF1A, PPARG, and PRKCA, act as drivers, whereas IL6, SRC, HIF1A, and AR act as suppressors, and PTGS2 is considered a marker.

The Nrf2 pathway, a classical ferroptosis regulatory pathway, correlates with GPX4 expression. Additionally, Nrf2-regulated HO-1 is involved in the regulation of GPX4 [26]. We hypothesized and experimentally verified the activation of the Nrf2 pathway during VA intervention in CAG (Fig. 7). Mechanistically, Nrf2 activation is suppressed by Keap1, a key negative regulator that facilitates its ubiquitination and degradation [27]. Our findings suggest that VA may modulate the Keap1-Nrf2 pathway, leading to increased Nrf2 nuclear translocation and the upregulation of downstream antioxidant targets (HO-1). Interestingly, KEGG analysis identified the PI3K-AKT pathway, which can activate Nrf2 in a non-Keap1-dependent manner [28]. We speculate that the multicomponent nature of VA likely involves multiple components and pathways involved in Nrf2 activation and requires further research.

Although our integration of network pharmacology partially addresses this complexity, some limitations remain. Our focus on the small-molecule

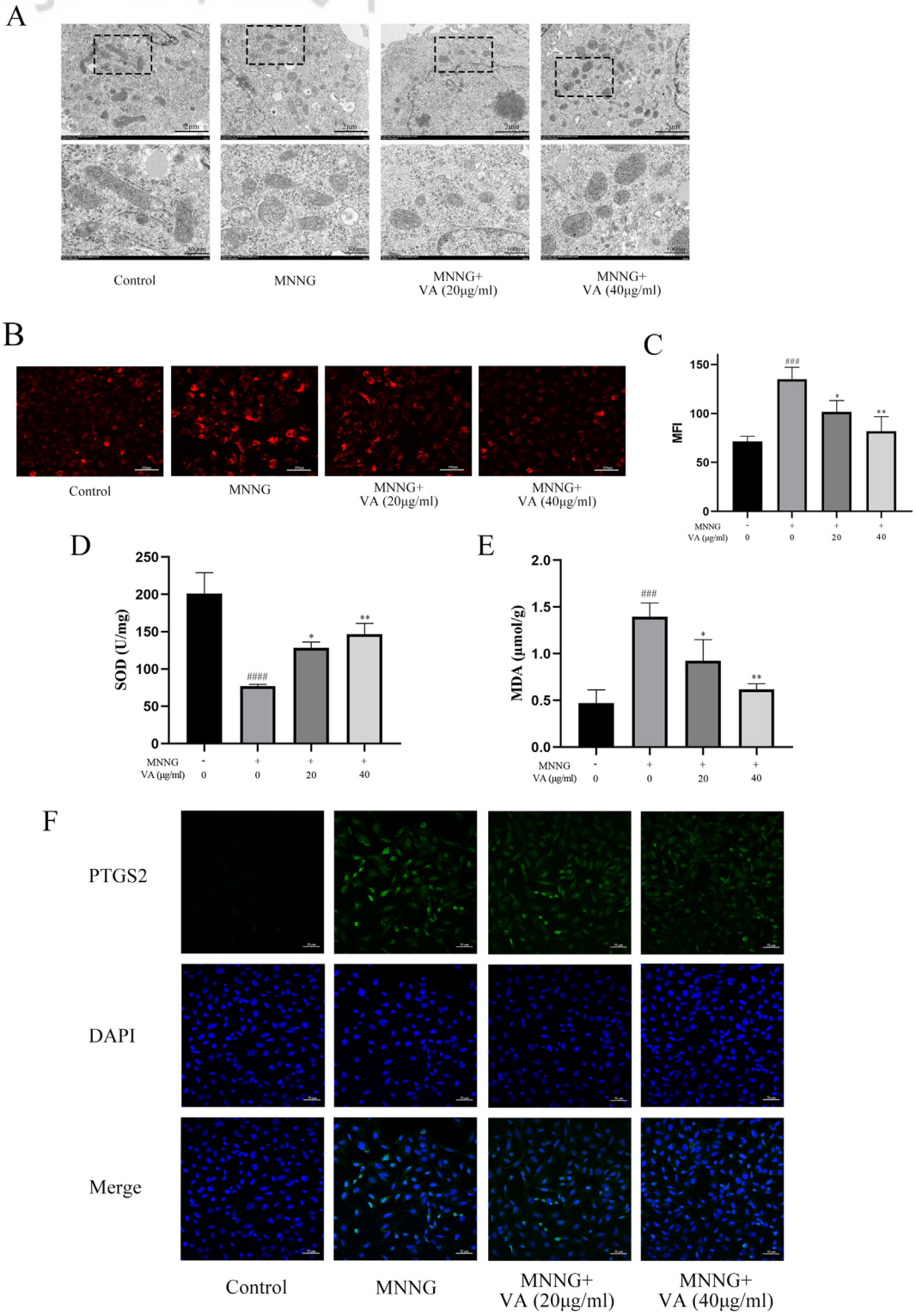

Fig. 5. Effects of VA on MNNG-induced oxidation and ferroptosis in vitro. (A) TEM images of mitochondria. The upper row represents low magnification, and the lower row shows high magnification. (B–C) Ferrous ions by ferroOrange. (D–E) The levels of SOD and MDA. (F) PTGS2 expression by immunofluorescence.

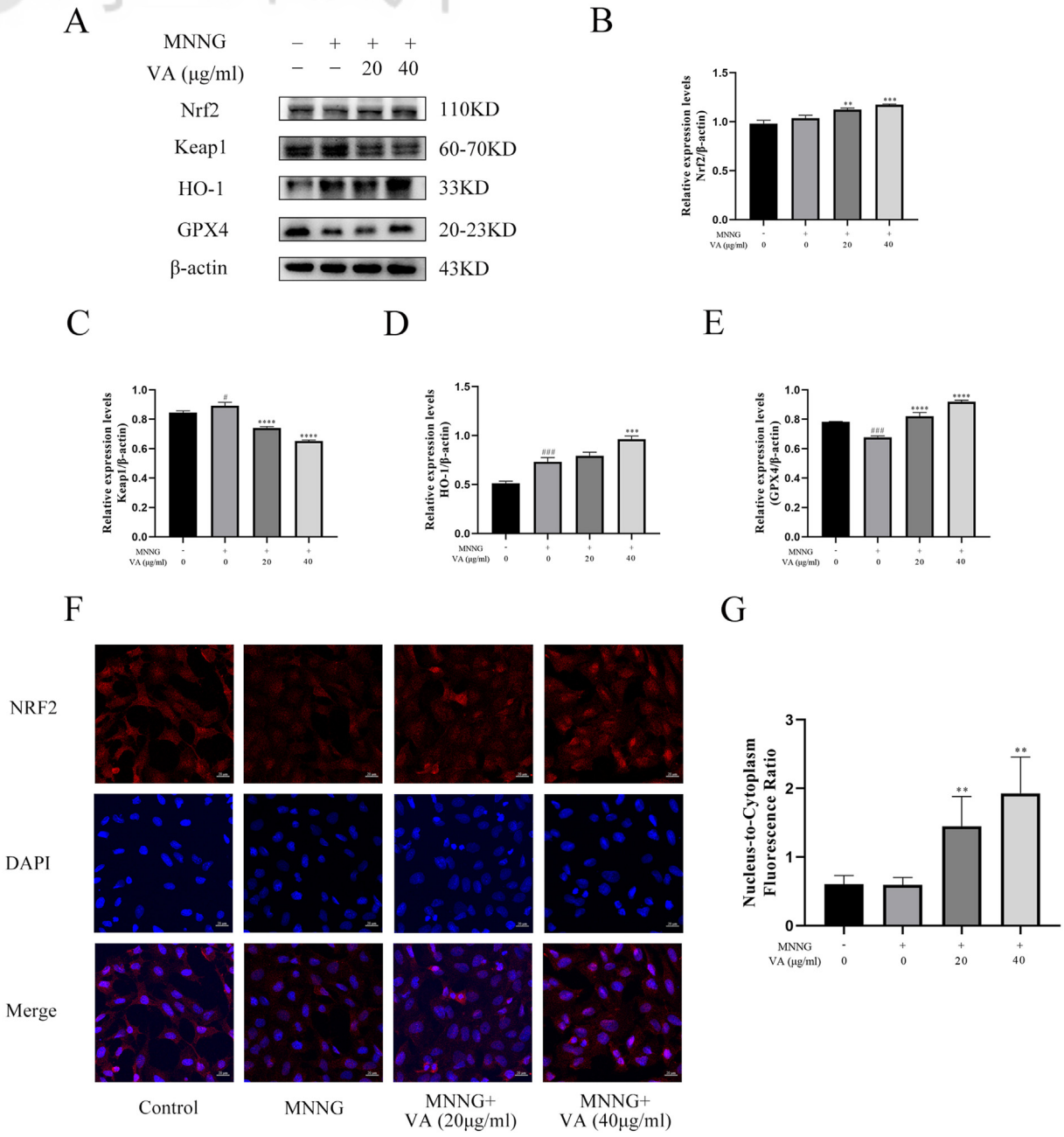

Fig. 6. Effects of VA on Keap1-Nrf2/HO-1/GPX4 pathway. (A) The expression of proteins. (B–E) Bar graphs of relative protein expression (n = 3). (F) Nrf2 expression by immunofluorescence. (G) Nrf2 nucleus-to-cytoplasm fluorescence ratio.

components of VA overlooked the potential role of peptides, which may have influenced subsequent analyses. Additionally, further screening and confirmation of the key compounds in CAG, along with molecular docking results highlighting potential key molecules, are necessary. Future experiments should further explore the pharmacological effects and mechanisms.

In conclusion, our study elucidated the therapeutic potential of VA for CAG treatment through ferroptosis-related mechanisms, bridging network pharmacology, and experimental validation. This work not only sheds light on the therapeutic mechanisms of VA but also paves the way for exploring natural complex ingredient drugs in disease treatment.

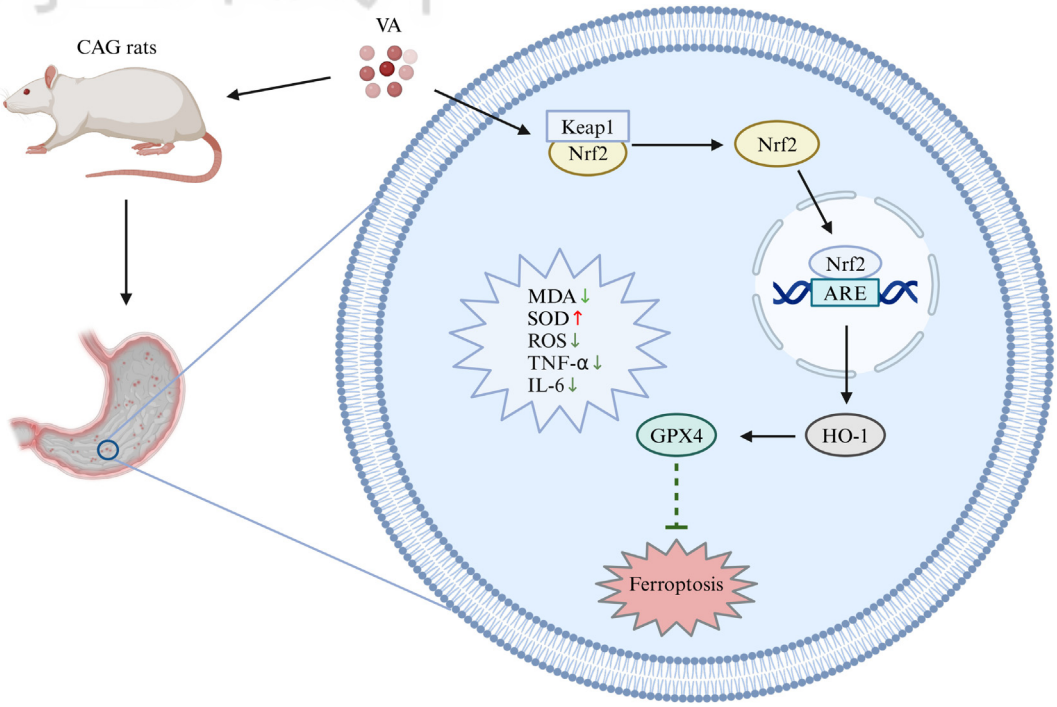

Fig. 7. Possible mechanism of the protective effects of VA on CAG.

Author contributions

QL: Conceptualization, Data curation, Formal analysis, Investigation, Methodology, Software, Validation, Visualization, Writing – original draft. ZG: Investigation, Methodology, Writing – review & editing. CD: Conceptualization, Validation, Writing – review & editing. RZ: Conceptualization, Validation, Writing – review & editing. GL: Conceptualization, Funding acquisition, Methodology, Project administration, Resources, Supervision, Validation, Writing – review & editing.

Data availability statement

The original contributions presented in the study are included in the article or supplementary material. Further inquiries can be directed to the corresponding author.

Funding

This work was supported by a grant from The National Natural Science Foundation of China (Grant No. 81870388).

Conflict of interest

The authors declare that the research was conducted in the absence of any commercial or financial relationships that could be construed as a potential conflict of interest.

References

[1] Shah SC, Piazuelo MB, Kuipers EJ, Li D. AGA clinical practice update on the diagnosis and management of atrophic gastritis: expert review. Gastroenterology 2021;161:1325–13232e7.
[2] Vannella L, Lahner E, Bordi C, Pilozzi E, Di Giulio E, Corleto VD, et al. Reversal of atrophic body gastritis after H. pylori eradication at long-term follow-up. Dig Liver Dis 2011;43:295–9.
[3] Piazuelo MB, Bravo LE, Mera RM, Camargo MC, Bravo JC, Delgado AG, et al. The Colombian chemoprevention trial: 20-year follow-up of a cohort of patients with gastric precancerous lesions. Gastroenterology 2021;160:1106–11017e3.
[4] Dixon SJ, Lemberg KM, Lamprecht MR, Skouta R, Zaitsev EM, Gleason CE, et al. Ferroptosis: an iron-dependent form of nonapoptotic cell death. Cell 2012;149:1060–72.
[5] Liu M, Kong XY, Yao Y, Wang XA, Yang W, Wu H, et al. The critical role and molecular mechanisms of ferroptosis in antioxidant systems: a narrative review. Ann Transl Med 2022;10:368.
[6] Liu K, Huang H, Xiong M, Wang Q, Chen X, Feng Y, et al. IL-33 accelerates chronic atrophic gastritis through AMPK-ULK1 axis mediated autolysosomal degradation of GKN1. Int J Biol Sci 2024;20:2323–38.
[7] Zhang N, Chen P, Liang X, Sun J, Liu Q, Guan S, et al. Luteolin targets the AGE-RAGE signaling to mitigate inflammation and ferroptosis in chronic atrophic gastritis. Aging (Albany NY) 2024;16:10918–30.
[8] Zhao Y, Zhao J, Ma H, Han Y, Xu W, Wang J, et al. High hepcidin levels promote abnormal iron metabolism and ferroptosis in chronic atrophic gastritis. Biomedicines 2023;11:2338.
[9] Guo Y, Jia X, Du P, Wang J, Du Y, Li B, et al. Mechanistic insights into the ameliorative effects of Xianglianhuazhuo formula on chronic atrophic gastritis through ferroptosis mediated by YY1/miR-320a/TFRC signal pathway. J Ethnopharmacol 2024;323:117608.
[10] Sui Z, Zhang L, Huo Y, Zhang Y. Bioactive components of velvet antlers and their pharmacological properties. J Pharm Biomed Anal 2014;87:229–40.

[11] Lee SH, Yang HW, Ding Y, Wang Y, Jeon YJ, Moon SH, et al. Anti-inflammatory effects of enzymatic hydrolysates of velvet antler in RAW 264.7 cells in vitro and zebrafish model. EXCLI J 2015;14:1122–32.
[12] Dong Y, Liu L, Shan X, Tang J, Xia B, Cheng X, et al. Pilose antler peptide attenuates LPS-induced inflammatory reaction. Int J Biol Macromol 2018;108:272–6.
[13] Wang X, Li H, Liu Y, Wu H, Wang H, Jin S, et al. Velvet antler methanol extracts (MEs) protects against oxidative stress in Caenorhabditis elegans by SKN-1. Biomed Pharmacother 2020;121:109668.
[14] Zheng K, Li Q, Lin D, Zong X, Luo X, Yang M, et al. Peptidomic analysis of pilose antler and its inhibitory effect on triple-negative breast cancer at multiple sites. Food Funct 2020;11:7481–94.
[15] Hao M, Peng X, Sun S, Ding C, Liu W. Chitosan/sodium alginate/velvet antler blood peptides hydrogel promoted wound healing by regulating PI3K/AKT/mTOR and SIRT1/NF-kappaB pathways. Front Pharmacol 2022;13:913408.
[16] Liu Y, Li H, Li Y, Yang M, Wang X, Peng Y. Velvet antler methanol extracts ameliorate Parkinson's disease by inhibiting oxidative stress and neuroinflammation: from C. elegans to mice. Oxid Med Cell Longev 2021;2021:8864395.
[17] Zhou W, Zhang H, Wang X, Kang J, Guo W, Zhou L, et al. Network pharmacology to unveil the mechanism of Moluodan in the treatment of chronic atrophic gastritis. Phytomedicine 2022;95:153837.
[18] Sun Y, Wen X, Li Z, Xu L, Xia M. Integrated network pharmacology and proteomics to reveal the cognitive improvement effect of Wuzang Wenyang Huayu decoction on vascular dementia. Chin Med J (Engl) 2022;135:2380–2.
[19] Janhavi P, Divyashree S, Sanjailal KP, Muthukumar SP. DoseCal: a virtual calculator for dosage conversion between human and different animal species. Arch Physiol Biochem 2022;128:426–30.
[20] Chen M, Zhong G, Liu M, He H, Zhou J, Chen J, et al. Integrating network analysis and experimental validation to reveal the mitophagy-associated mechanism of Yiqi Huoxue (YQHX) prescription in the treatment of myocardial ischemia/reperfusion injury. Pharmacol Res 2023;189:106682.
[21] Yang WS, SriRamaratnam R, Welsch ME, Shimada K, Skouta R, Viswanathan VS, et al. Regulation of ferroptotic cancer cell death by GPX4. Cell 2014;156:317–31.
[22] Thrift AP, Wenker TN, El-Serag HB. Global burden of gastric cancer: epidemiological trends, risk factors, screening and prevention. Nat Rev Clin Oncol 2023;20:338–49.
[23] Liu F, Nong X, Qu W, Li X. Weikangling capsules combined with omeprazole ameliorates ethanol-induced chronic gastritis by regulating gut microbiota and EGF-EGFR-ERK pathway. Life Sci 2023;315:121368.
[24] Wen J, Wu S, Ma X, Zhao Y. Zuojin Pill attenuates Helicobacter pylori-induced chronic atrophic gastritis in rats and improves gastric epithelial cells function in GES-1 cells. J Ethnopharmacol 2022;285:114855.
[25] Liu Y, Wan Y, Jiang Y, Zhang L, Cheng W. GPX4: the hub of lipid oxidation, ferroptosis, disease and treatment. Biochim Biophys Acta Rev Cancer 2023;1878:188890.
[26] Dang R, Wang M, Li X, Wang H, Liu L, Wu Q, et al. Edaravone ameliorates depressive and anxiety-like behaviors via Sirt1/Nrf2/HO-1/Gpx4 pathway. J Neuroinflammation 2022;19:41.
[27] Yamamoto M, Kensler TW, Motohashi H. The KEAP1-NRF2 system: a thiol-based sensor-effector apparatus for maintaining redox homeostasis. Physiol Rev 2018;98:1169–203.
[28] Yu C, Xiao JH. The Keap1-Nrf2 system: a mediator between oxidative stress and aging. Oxid Med Cell Longev 2021;2021:6635460.